LASER INTERFEROMETER GRAVITATIONAL WAVE OBSERVATORY
- LIGO -
CALIFORNIA INSTITUTE OF TECHNOLOGY
MASSACHUSETTS INSTITUTE OF TECHNOLOGY

Technical Note	**LIGO-T970101-B – D**	5/6/97 3/13/03

Strain Calibration in LIGO

Daniel Sigg

Distribution of this draft:

ISC

This is an internal working note
of the LIGO Project.

California Institute of Technology
LIGO Project - MS 51-33
Pasadena CA 91125
Phone (818) 395-2129
Fax (818) 304-9834
E-mail: info@ligo.caltech.edu

Massachusetts Institute of Technology
LIGO Project - MS 20B-145
Cambridge, MA 01239
Phone (617) 253-4824
Fax (617) 253-7014
E-mail: info@ligo.mit.edu

WWW: http://www.ligo.caltech.edu/

1 INTRODUCTION

This document discusses the gravitational wave strain calibration in LIGO. Section 2 shows that requirements of ~2% in amplitude and ~10μsec in the determination of the arrival time will be of sufficient accuracy for most of the physics derived from early detections. Section 3 summarizes the interaction of a gravitational wave with the LIGO interferometer and gives formulas which connect the measured antisymmetric port signal with the strain of a gravitational wave. Section 4 includes the longitudinal servo system in the analysis and Section 5 describes a possible calibration actuator based on the momentum transfer of photons. Section 6 works out three different calibration procedures: swept sine, permanent calibration lines and the addition of a wide-bandwidth pseudo-random signal.

2 CALIBRATION REQUIREMENTS

The requirements for the gravitational wave strain calibration in LIGO are based on the assumption that if one detects a few events (1 – 10) with reasonable signal-to-noise ratios (10 – 100), the deduced (astro-) physical results should not be limited by systematic uncertainties in the detector, but rather by the random noise sources of the interferometer — i.e., seismic noise, thermal noise and photon count statistics. As shown below an amplitude calibration with an accuracy of ±2% and an absolute timing precision (relative to world time) of ±10μsec would most likely be adequate.

2.1 AMPLITUDE CALIBRATION

2.1.1 Distance from the Source

Since one can extract the chirp mass of a binary system from the rate the frequency changes with time, one is able to make a prediction of the binary's absolute gravitational luminosity [1]. That means that a measurement of the amplitude of the signal measured on Earth is enough to determine the distance to the source. Because the measured amplitude is inversely proportional to the distance, a relative amplitude measurement error will directly propagate into an uncertainty of the distance. A gain calibration error would enter as a system error. Requiring a 2% calibration accuracy guarantees that the statistical uncertainty dominates the error budget for signal-to-noise ratios at and below ~30.

2.1.2 Matched Filter Analysis

The measured signal-to-noise ratio of the classical matched filter analysis turns out to be first order insensitive in the calibration of the gain [2]. This can be readily understood by recognizing that a calibration error will affect both the signal level and the noise level the same way and, therefore, cancel out in the signal-to-noise ratio.

2.2 TIMING CALIBRATION

2.2.1 Coincidence

For detectors far away the coincidence interval for a signal coming from an arbitrary direction is determined by the light travel time between the detectors. The two LIGO sites are separated by 10ms which is much larger than any sensible timing resolution.

The signal-to-noise ratio of a sinusoidal signal of duration T can be estimated by

$$\frac{1}{R_{S/N}} \approx \frac{h_N}{h_S}\frac{1}{\sqrt{2T}} \tag{1}$$

where h_S and h_N are the signal and the noise amplitudes respectively. If the frequency of the signal is f_0 the timing uncertainty approximately becomes

$$\Delta t \approx \frac{1}{2\pi f_0}\frac{h_N}{h_S}\frac{1}{\sqrt{2T}} \approx \frac{1}{2\pi f_0}\frac{1}{R_{S/N}} \tag{2}$$

For two nearby interferometers tuned to detect correlated events with a signal-to-noise ratio of 10 or better at frequencies around 150Hz the systematic timing error should be well below 100μsec.

2.2.2 Localization on the Sky

Fig. 1 shows a gravitational wavefront propagating through two detectors separated by a distance *L*. The incident angle β (angle of the cone in 3 dimensions) is given by the difference in the time of arrival τ as follows:

$$\sin\beta = \frac{c\tau}{L} \tag{3}$$

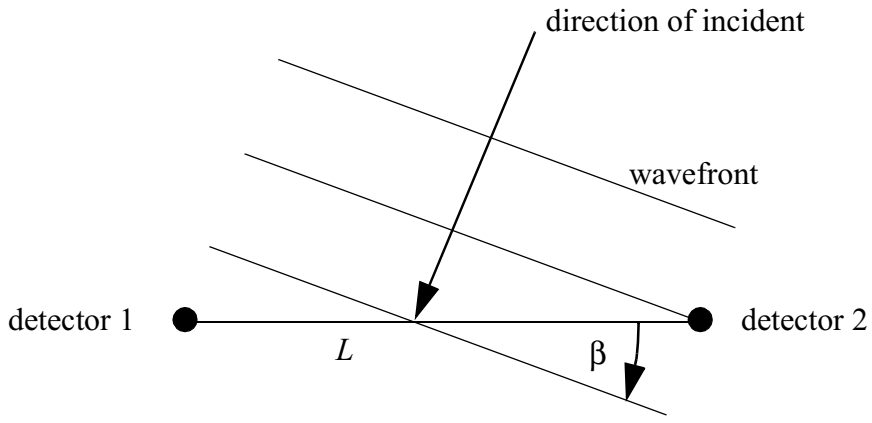

Figure 1: Gravitational wavefront as seen by two detectors.

and the angular uncertainty becomes

$$\Delta\beta = \frac{1}{\cos\beta}\frac{c\Delta\tau}{L} \tag{4}$$

For a separation of $L/c \approx 10\,\mathrm{ms}$ and a timing error of $10\,\mu\mathrm{sec}$ the angular uncertainty close to normal incidence is roughly 3 arcmin. Using eqn. (2) to estimate the required signal-to-noise ratio of such an event yields, e.g., $R_{S/N} \approx 100$ at 150 Hz, or $R_{S/N} \approx 15$ at 1 kHz.

2.2.3 Periodic Sources

The search for periodic sources involves long observation times, but as long as the signal-to-noise ratio is not significantly larger than the detection threshold the requirements placed on the gain calibration accuracy are not severe. Contamination of the arm cavity mirrors over time will reduce the arm cavity storage time and, therefore, move the arm cavity pole to higher frequencies. This in turn will introduce a phase shift in the measured signal at the antisymmetric port. On a short time scale this effect will be small enough, so that the signal-to-noise ratio is not significantly deteriorated. On longer time scales the periodic calibration runs can be used for correcting the phase if necessary. Absolute timing accuracy is not as relevant as for faster events, since the position on the sky can be deduced from the applied Doppler corrections rather than the time of arrival.

2.2.4 Matched Filter Analysis

The measured signal-to-noise ratio of the classical matched filter analysis turns out to be first order insensitive in the calibration of the phase [2]. Since these filters are scanned over all arrival times to find the best match, a simple time delay is irrelevant. On the other hand a dispersive effect due to a frequency dependent phase error will change the shape of burst signals or chirp signals and, thus, give rise to a (second order) change in the signal-to-noise ratio.

3 Gravitational Wave Interaction with an Interferometric Detector

3.1 The Coordinate System

We chose the coordinate system to be aligned with the two arms of the interferometer, where the origin is positioned at the beamsplitter and the z-axis points vertically upwards (see Fig. 2).

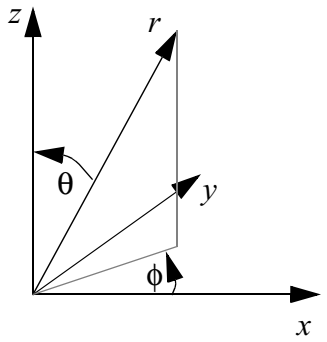

Figure 2: Coordinate System.

Spherical coordinates are defined by

$$r = \begin{bmatrix} r\sin\theta\cos\phi \\ r\sin\theta\sin\phi \\ r\cos\theta \end{bmatrix} \quad \text{with} \begin{cases} 0 \le \phi < 2\pi \\ 0 \le \theta < \pi \end{cases} \tag{5}$$

We then define the rotation operator $O(\theta, \phi)$ which rotates the z-axis in the direction of r:

$$O(\theta, \phi) = O(\phi)O(\theta) \tag{6}$$

$$\text{where } O(\phi) = \begin{bmatrix} \cos\phi & -\sin\phi & 0 \\ \sin\phi & \cos\phi & 0 \\ 0 & 0 & 1 \end{bmatrix} \quad \text{and} \quad O(\theta) = \begin{bmatrix} \cos\theta & 0 & \sin\theta \\ 0 & 1 & 0 \\ -\sin\theta & 0 & \cos\theta \end{bmatrix} \tag{7}$$

3.2 Round-Trip Phase Change

We write the phase of the light which it acquires in one round-trip in one of the interferometer arms as

$$\Phi_{rt}(t_0) = \int_{t_0}^{t_0 + t(2L)} \omega \, dt \tag{8}$$

where L is the length of the arm, ω is the angular frequency of the light and t_0 the time the photon leaves the origin. We now change the integration over time into one over length by using

$$d\tau^2 = dx_\mu g_{\mu\nu} dx^\nu = 0 \quad \text{with } g_{\mu\nu} = \eta_{\mu\nu} + h_{\mu\nu} \tag{9}$$

where $\eta_{\mu\nu}$ is the Minkovski metric and $h_{\mu\nu}$ is the space-time ripple due to the gravitational wave [3]. For a gravitational wave traveling along the z-axis $h_{\mu\nu}$ in the transverse-traceless gauge becomes

$$h_{\mu\nu} = \cos(\Omega t - kz) \left[\begin{array}{c|ccc} 0 & 0 & 0 & 0 \\ \hline 0 & & & \\ 0 & & \hat{H}_{ik} & \\ 0 & & & \end{array}\right] \quad \text{with } \hat{H}_{ik} = \begin{bmatrix} h_+ & h_\times & 0 \\ h_\times & -h_+ & 0 \\ 0 & 0 & 0 \end{bmatrix} \tag{10}$$

where Ω is the angular frequency of the gravitational wave, k is its wave vector, h_+ and $h_\times$ are the wave amplitudes for the "+" and the "×" polarization, respectively.

For arbitrary directions one has to rotate both z and H_{ik} in the direction of the wave vector k.

$$kz \to k(k_x x + k_y y + k_z z) \quad \text{with} \begin{cases} k_x = \sin\theta\cos\phi \\ k_y = \sin\theta\sin\phi \\ k_z = \cos\theta \end{cases} \tag{11}$$

$$\hat{H}_{ik} \to H_{ik} = O(\theta, \phi)\hat{H}_{ik}O(\theta, \phi)^{-1} \equiv \begin{bmatrix} h_{xx} & h_{xy} & h_{xz} \\ h_{yx} & h_{yy} & h_{yz} \\ h_{zx} & h_{zy} & h_{zz} \end{bmatrix} \tag{12}$$

For an integration along the x-axis or the y-axis h_{xx} and h_{yy} are the only relevant matrix elements, respectively.

$$h_{xx} = -\cos\theta \sin 2\phi \, h_\times + (\cos^2\theta \cos^2\phi - \sin^2\phi) h_+ \tag{13}$$

$$h_{yy} = \cos\theta \sin 2\phi \, h_\times + (\cos^2\theta \sin^2\phi - \cos^2\phi) h_+ \tag{14}$$

Fig. 3 shows the angular dependence of $|h_{xx} - h_{yy}|$ for both polarizations and their square-sum average. Using eqn. (9) we rewrite eqn. (8) as

$$\Phi^x_{rt}(t_0) = \frac{\omega}{c}\int_0^L \{\sqrt{1 + h_{xx}\cos(\Omega t_0 + k(1-k_x)x)} + \sqrt{1 + h_{xx}\cos(\Omega t_0 + k(2L-(1+k_x)x))}\}\, dx \tag{15}$$

Similarly, $\Phi^y_{rt}(t_0)$ can be obtained by integrating along the *y*-axis. Since $h_{xx} \ll 1$ we can Taylor expand the square root of eqn. (15). Performing the integration, keeping only time-dependent terms, time-shift from departure to arrival, and changing to a complex notation where the absolute value denotes the amplitude and the argument denotes the phase shift, one gets:

$$\Delta\Phi^x_{rt} = \frac{h_{xx}L\omega}{c} e^{-i\Phi_\Omega} \frac{\sin\Phi_\Omega + ik_x\cos\Phi_\Omega - ik_x e^{-ik_x\Phi_\Omega}}{\Phi_\Omega(1-k_x^2)} \tag{16}$$
$$\approx \frac{h_{xx}L\omega}{c}\,\mathrm{sinc}\,\Phi_\Omega \cos\left(\frac{k_x\Phi_\Omega}{\sqrt{12}}\right) e^{-i(1+k_x/2)\Phi_\Omega}$$

where $\Phi_\Omega = L\Omega/c$. The approximation yields the exact solution for a gravitational wave traveling along the *z*-axis. For all directions we assume $\Phi_\Omega \ll 1$. From eqn. (16) one sees that the signal delay for photons arriving at the origin is $1 + k_x/2$ times half the round-trip time. The finite time a photon spends in a Michelson arm also leads to a small correction of the signal amplitude which would otherwise be determined by $h_{xx}L$ only. Fig. 4 shows the amplitude correction and time delay of the round trip phase of a gravitational wave as function of k_x relative to one of normal incident and strength h_{xx}. These effects are generally small and in most cases negligible.

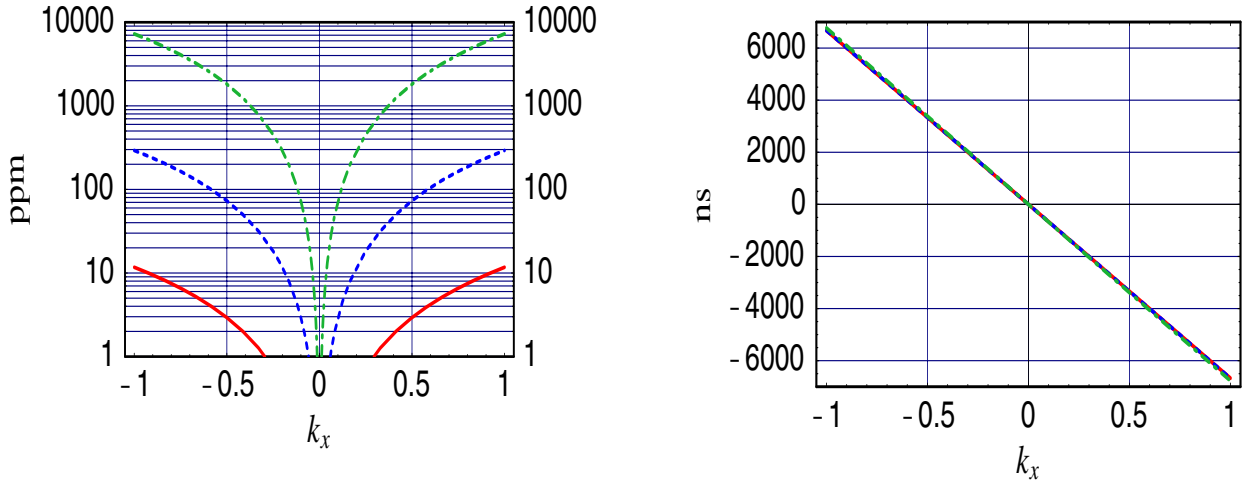

Figure 4: Amplitude correction (left) and time delay of a gravitational wave with non-normal incident and frequencies of 200 Hz (solid curve), 1000 Hz (dashed) and 5000 Hz.

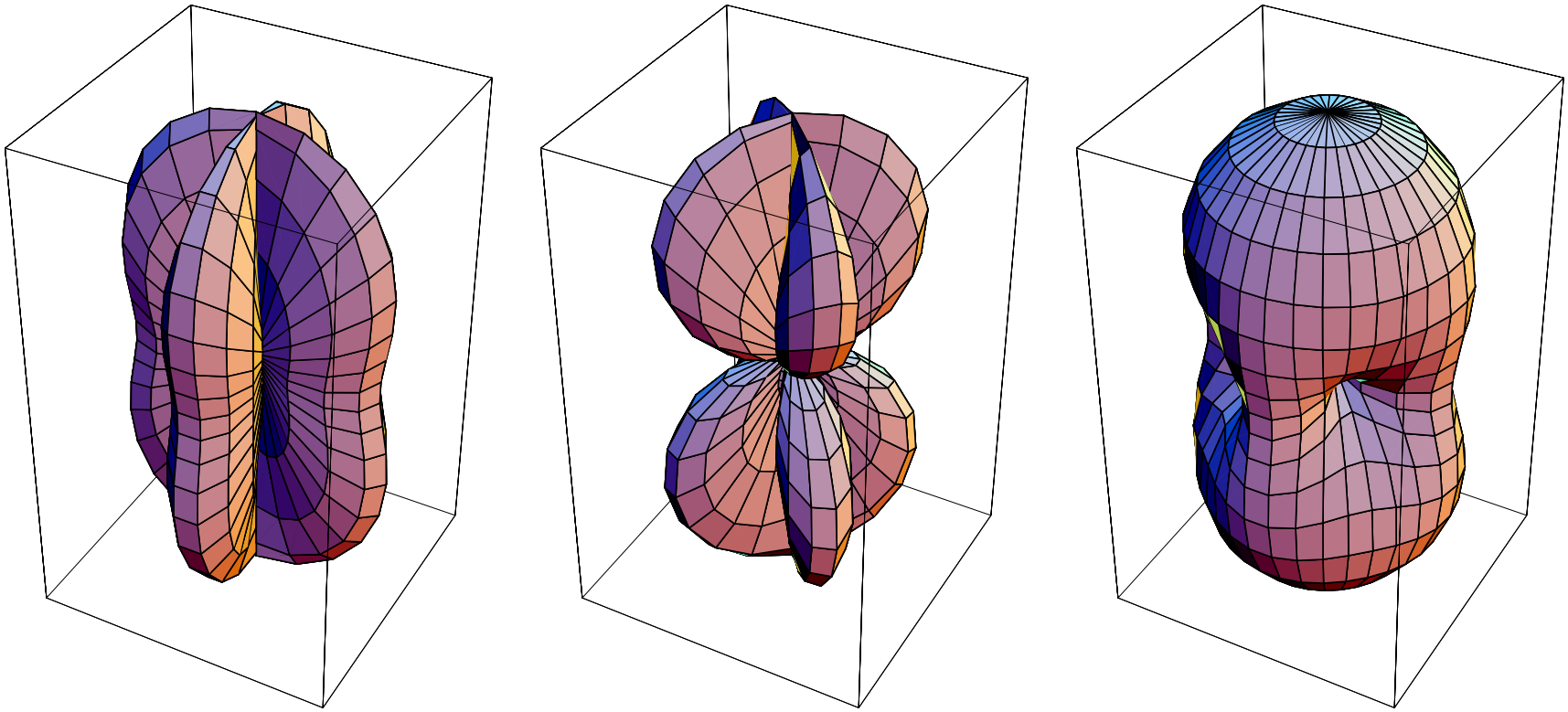

Figure 3: ***h*** **sensitivity as function of angle for the "+" polarization, the "×" polarization and the averaged polarization.**

3.3 HIGHER FREQUENCY RESPONSE

It is useful to calculate the antenna pattern at higher frequencies. Since the arm cavities have a displacement response that is periodic in frequency and repeats itself every free-spectral-range, one might assume that response to gravitational waves follows this pattern. In particular, the displacement sensitivity of a Fabry-Perot cavity is as good at multiples of the free-spectral range as it is at dc. However, at the free-spectral-range frequency the antenna length is also a multiple of a half-wave length of the gravitational wave. Using the variables of eqn. (16) we can write:

$$\Omega = 2\pi m f_{FSR} = 2\pi m \frac{c}{2L} \quad \Rightarrow \quad \Phi_\Omega = \pi m \tag{17}$$

This in turn will result in a zero of the term proportional to $\mathrm{sinc}\Phi_\Omega$ in the second line of eqn. (16), and may look like the response of a Fabry-Perot cavity to gravitational wave at the free-spectral-range frequency is identical zero. But, it was first recognized in ref. [5] that this is not true for all directions. Going back to the first line of eqn. (16) we see that for non-zero k_x the second and third term in the numerator will not vanish at the free-spectral-range. In Fig. 5 we show the angular dependency of the sensitivity $|H_{FSR}|$ for both polarizations and their square-sum average when the antenna length is $\lambda/2$. The boxes shown in this figure are roughly an order of magnitude smaller than the ones in Fig. 3. The sensitivity at the first free-spectral-range can be simplify to:

$$H_{FSR} = \frac{h_{xx}(1+e^{-i\pi k_x})ik_x}{\pi(1-k_x^2)} - \frac{h_{yy}(1+e^{-i\pi k_y})ik_y}{\pi(1-k_y^2)} \tag{18}$$

The polarization patterns are obtained as follows:

$$H_+ = H_{FSR}\big|_{h_\times = 0,\ h_+ = 1}, \quad H_\times = H_{FSR}\big|_{h_\times = 1,\ h_+ = 0} \quad \text{and} \quad \bar{H} = \sqrt{|H_+|^2 + |H_\times|^2} \tag{19}$$

To estimate the overall loss of sensitivity at the free-spectral range frequency we can compute the volume of the corresponding antenna pattern and compare it with the volume of the "peanut". The volume integral can be written as

$$V = \int_0^{2\pi} d\phi \int_0^{\pi} d\theta \int_0^{|H(\phi,\theta)|} dr\, r^2 \sin\theta\,. \tag{20}$$

For the ratio of volumes $V(\Phi_\Omega = \pi)/V(\Phi_\Omega = 0)$ we obtain a factor of about $1/150$. Or, in other words the average range that a source can be seen is about a factor of 5.3 smaller at the first free-spectral-range frequency than at dc (assuming all other factors being equal).

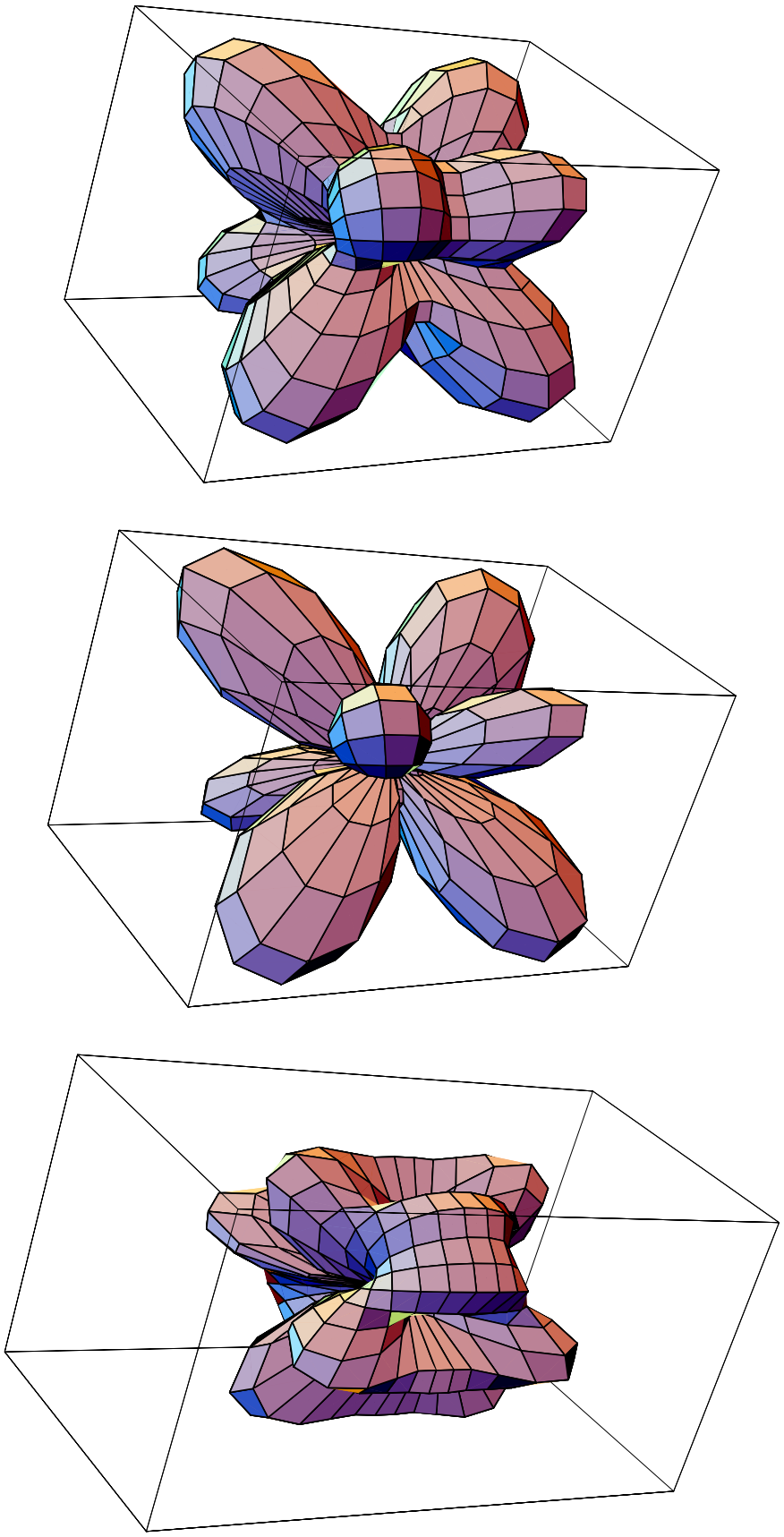

Figure 5: ***h*** **sensitivity for arm length λ/2 as function of angle for the "+" polarization, the "×" polarization and the averaged polarization.**

3.4 Arm Cavity Response and antisymmetric Port Signal

To calculate the response of a cavity to a gravitational wave of a certain frequency Ω we write the electric field as a three-component vector denoting the carrier field, the upper audio sideband and the lower audio sideband. The round-trip operator $X(\Omega)$ can be expressed as [4]

$$X(\Omega) = \begin{bmatrix} 1 & 0 & 0 \\ -\frac{i}{2}\Delta\Phi_{rt} & e^{-2i\Omega L/c} & 0 \\ -\frac{i}{2}\Delta\Phi_{rt}^{*} & 0 & e^{2i\Omega L/c} \end{bmatrix} \tag{21}$$

where we neglected the factor $e^{-2i\omega L/c + 2i\eta}$ which is unity when the cavity is on resonance (with η the Guoy phase shift). The reflected field operator for a cavity then becomes

$$X_{refl}(\Omega) = [r_1 - (r_1^2 + t_1^2)\sqrt{1-\delta}X(\Omega)][1 - r_1\sqrt{1-\delta}X(\Omega)]^{-1} \tag{22}$$

where r_1 and t_1 are the amplitude reflectivity and transmission coefficients of the input mirror and δ is the total round-trip loss (including the reflectivity of the rear mirror). Using a carrier only the input field E_{in}, the reflected audio sidebands are

$$E_{refl}^{+\Omega} = \frac{i}{2}G_{refl}(\Omega)\Delta\Phi_{rt}e^{i\Omega t}E_{in} \quad \text{and} \quad E_{refl}^{-\Omega} = \frac{i}{2}G_{refl}^{*}(\Omega)\Delta\Phi_{rt}^{*}e^{-i\Omega t}E_{in} \tag{23}$$

$$\text{with} \quad G_{refl}(\Omega) = \frac{\sqrt{1-\delta}\,t_1^2}{(1-\sqrt{1-\delta}r_1)(1-\sqrt{1-\delta}r_1e^{-2i\Omega L/c})} \tag{24}$$

$$\approx \frac{\sqrt{1-\delta}\,t_1^2}{(1-\sqrt{1-\delta}\,r_1)^2}\,\frac{e^{i\Omega L/c}}{1+i\frac{\Omega}{\omega_{cav}}} \qquad \text{for } \Omega \ll \frac{c}{2L}$$

and with the cavity pole at $\omega_{cav} = \dfrac{1-r_1\sqrt{1-\delta}}{\sqrt{r_1\sqrt{1-\delta}}}$. (25)

The audio sideband signal can be simplified to

$$E_{refl}^{+\Omega} + E_{refl}^{-\Omega} = |G(\Omega)\Delta\Phi_{rt}|\cos(\Omega t + \arg(G(\Omega)\Delta\Phi_{rt}))E_{in} \equiv |g|\cos(\Omega t + \arg g) \tag{26}$$

The signal at the antisymmetric port is then given by

$$E_{dark} = it_{bs}r_{bs}\{\sqrt{1-\delta_x}g_x\cos(\Omega t + \arg g_x) - \sqrt{1-\delta_y}g_y\cos(\Omega t + \arg g_y)\}E_{RC} \tag{27}$$

where r_{bs} and t_{bs} are the amplitude reflectivity and transmission coefficients for the beamsplitter, respectively, δ_x and δ_y are the losses in the (short) inside Michelson arms for the incident carrier light and the reflected gravitational wave signal, g_x and g_y denote the signals from the in-line and

the off-line arm cavities, respectively, and E_{RC} is the carrier field incident on the beamsplitter. We now write the rf sideband signal at the antisymmetric port as

$$E_{dark}^{sb} = 2i|E_{sb}|\sin\omega_m t \tag{28}$$

where $|E_{sb}|$ is the field strength of either rf sideband and ω_m is the angular modulation frequency. Down-converting the signal yields

$$\begin{aligned} V_{dark} &= R\sin\omega_m t\ \varepsilon_{PD}\left|E_{dark}^{sb} + E_{dark}\right|^2 \\ &\overset{dc}{=} \sqrt{32}R\ \varepsilon_{PD}\sqrt{P_{RC}P_{sb}}\,t_{bs}r_{bs}\{\sqrt{1-\delta}_x G_x(\Omega)\Delta\Phi_{rt}^x - \sqrt{1-\delta}_y G_y(\Omega)\Delta\Phi_{rt}^y\} \end{aligned} \tag{29}$$

On the last line we returned to the complex notation where the absolute value denotes the signal amplitude and where the argument denotes the signal phase shift. R is the transimpedance gain of the mixer/filter/amplifier circuit, ε_{PD} is the efficiency of the photodetector, P_{RC} and P_{sb} are the carrier power on the beamsplitter and the total sideband power at the antisymmetric port, respectively.

4 Servo System Response

4.1 Quantization Effects

An analog-to-digital converter will generally add a time delay of half the sampling period. In order to keep the uncertainty in this correction negligible, the sampling period must not be significantly larger than the desired timing resolution. Anti-aliasing filters or a slow settling time of the preceding amplifier may contribute to additional delays.

4.2 Crosscoupling from Other Degrees-of-Freedom

The beamsplitter clearly separates differential from common mode changes. Hence, we only have to consider the small inside Michelson length as a possible source of crosscoupling. Since for the initial LIGO the unity gain frequency of the small Michelson loop will be below the gravitational wave detection band a small Michelson length change will couple unattenuated into the antisymmetric port signal. For a gravitational wave this coupling is suppressed by roughly a factor equal to half the finesse of the arm cavity times the ratio of the length between beamsplitter and input mirror over the cavity length.

$$\Delta L_{\text{meas}} \approx \left(1 + \frac{2l}{FL}\right)\Delta L_{gw} \tag{30}$$

For the present configuration this factor is of order 3×10^{-5}.

4.3 Reconstructing the Gravitational Wave Signal

The unity gain frequency of the differential arm length servo may be lying inside the gravitational wave detection band. In principle, the gravitational wave signal is best determined from the

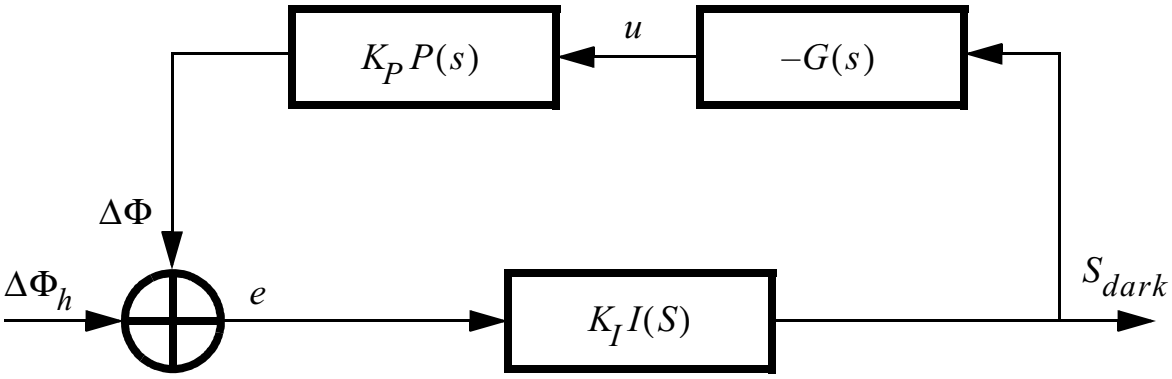

Figure 6: Servo loop model for differential arm length control. The gravitational wave signal $\Delta\Phi_h$ is added to the signal $\Delta\Phi$ coming from the suspended test mass $P(s)$ to give the error signal e which is turned into the antisymmetric port signal S_{dark} by the interferometer $I(s)$. The controller is described by $G(s)$ and produces the control signal u. The constants K are additional gains; they are mainly introduced to account for gain errors and are nominal unity.

control signal below the unity gain frequency, from the error signal above the unity gain frequency and from a combination of both signals around the unity gain frequency. However, for a digital servo the transfer function between the error signal and the control signal is known to a very high precision and, therefore, no additional information is gained by looking at the control signal. Since the crosscoupling from the Michelson servo is negligible, one can perform the reconstruction of the gravitational wave signal with a one dimensional servo model (see Fig. 6). The closed loop response of the measured antisymmetric port signal S_{dark} as function of the gravitational wave induced round-trip phase $\Delta\Phi_h$ then becomes

$$S_{dark} = \frac{K_I I(s)}{1 + K_P K_I P(s) G(s) I(s)} \Delta\Phi_h \equiv GW(s)\Delta\Phi_h \tag{31}$$

Above the unity gain frequency the second term of the denominator in eqn. (31) is small compared to unity and the gain error is mainly given by the uncertainty in the optical/sensing gain K_I;. On the other hand, below the unity gain frequency the denominator is getting large and the gain error is dominated by the uncertainty in the controller gain K_P.

5 Photon Actuators

5.1 Momentum Transfer of Light

One way to calibrate the response of the interferometer is to apply a known force to the test masses and compare it to the measured signal at the antisymmetric port. One way is to use the coil drivers presently implemented in the suspension controllers. Since the bandwidth of the controller is fairly low, corrections for both the amplitude and the phase of the actuating signal have to be

taken into account. An other way to apply the force is to use an independent wideband actuator such as a laser beam. The recoil of the photons bounced off the mirror surface pushes the test mass by a small amount backwards. If the incident angle is α the applied force is

$$F = 2\cos\alpha\frac{h\nu}{c}\dot{N}_\gamma \tag{32}$$

where $\dot{N}_\gamma$ is the number of photons hitting the mirror per time. Expressing the photon rate in units of the light intensity P yields

$$\dot{N}_\gamma = \frac{P}{h\nu} \quad \Rightarrow \quad F = 2\cos\alpha\frac{P}{c} \tag{33}$$

Treating the test mass as a simple pendulum and writing the light intensity as

$$P(t) = P_0 + P\cos\omega_c t \tag{34}$$

the displacement amplitude of test mass can be written as

$$x_c(\omega_c) = 2\cos\alpha\,\frac{P}{cM}\,\frac{1}{\omega_p^2 - \omega_c^2 + i\omega_p\omega_c/Q} \approx -2\frac{\cos\alpha\,P}{cM\omega_c^2} \quad \text{for} \quad \omega_c \gg \omega_p \tag{35}$$

where ω_p and Q are the angular resonance frequency and the Q of the pendulum. As an example we take a laser with intensity $P \approx 10\,\text{mW}$, an incident angle close to normal and a test mass of $M \approx 10\,\text{kg}$, the displacement amplitude at $100\,\text{Hz}$ then becomes $x_c \approx 1.7\times10^{-17}\,\text{m}$.

5.2 Displacement Signal

The round-trip operator when the rear mirror is dithered with an amplitude x_c at an angular frequency ω_c is proportional to

$$\begin{bmatrix} 1 & 0 & 0 \\ 0 & e^{-i\Omega L/c} & 0 \\ 0 & 0 & e^{i\Omega L/c} \end{bmatrix} \begin{bmatrix} 1 & 0 & 0 \\ -i\frac{\omega}{c}x_c(\omega_c) & 1 & 0 \\ i\frac{\omega}{c}x_c(\omega_c) & 0 & 1 \end{bmatrix} \begin{bmatrix} 1 & 0 & 0 \\ 0 & e^{-i\Omega L/c} & 0 \\ 0 & 0 & e^{i\Omega L/c} \end{bmatrix} \tag{36}$$

$$= \begin{bmatrix} 1 & 0 & 0 \\ -i\frac{\omega}{c}x_c(\omega_c)e^{-i\Omega L/c} & e^{-2i\Omega L/c} & 0 \\ i\frac{\omega}{c}x_c(\omega_c)e^{i\Omega L/c} & 0 & e^{2i\Omega L/c} \end{bmatrix}$$

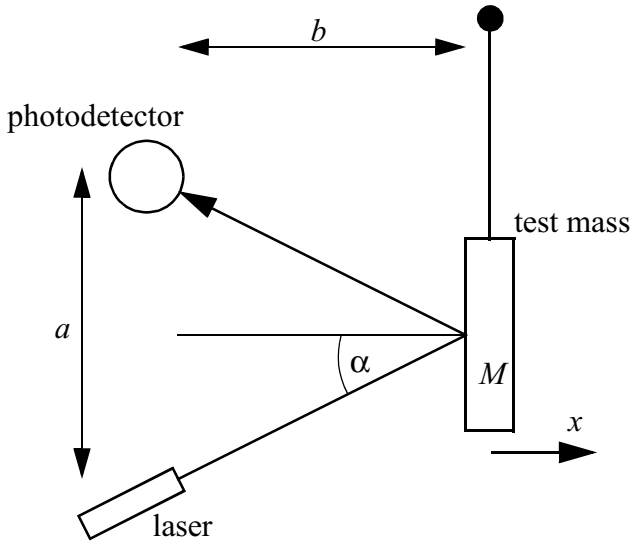

Figure 7: Possible setup of a photon actuator.

Comparing this with eqn. (21) — the round-trip operator for a gravitational wave — one can see that the time delay of the dithering signal of the rear mirror exactly corresponds to the one of a gravitational wave propagating along the *z*-axis and the following amplitude relation holds

$$x_c(\omega_c) \sim \frac{h_{xx}L}{2}\,\mathrm{sinc}\,\Phi_\Omega \tag{37}$$

Calculating the response to dithering the input mirror is more involved, since it introduces phase shifts both for the input field and for the round-trip field. Considering only the change of the cavity length the result is the same as for a rear mirror dither except an additional phase shift of $e^{i\Omega L/c}$. This can be naively understood by observing that moving the input mirror will immediately change the interference between the prompt reflected field and the transmitted field leaving the cavity. Additionally, dithering the input mirror changes the length of the small Michelson and, therefore, will generally produce an immediate signal at the antisymmetric port.

5.3 IMPLEMENTATION

A possible setup is shown in Fig. 7. The beam reflected from the mirror surface is guided to a photodetector which measures both amplitude and phase of the modulated laser light. This setup has the advantage that the precision of the applied force depends on the photodetector calibration and the incident angle only. In particular, the timing of the displacement dither can measured without unwanted signal delays if a higher bandwidth photodetector is used.

6 Calibration Procedures

We distinguish calibration procedures which take place during data runs and ones which take place when the detector is off-line. The first class of procedures will add additional signals to the gravitational wave detection band and, therefore, either degrade the overall sensitivity slightly or render certain discrete frequencies inaccessible. They have the advantage that they are performed concurrently with the data runs and, hence, are best suited when the sensitivity varies over time. Off-line calibration procedures, on the other hand, will add to the down-time of the detector, but will not degrade the gravitational wave sensitivity. They are best suited if the detector sensitivity is very stable over time and calibration runs are only required occasionally.

A calibration signal which is added during data runs has to be small enough not to deteriorate the gravitational wave sensitivity significantly. This can be achieved either by adding fixed frequency calibration lines or by adding a wideband pseudo-random signal. In both cases the actuation is known and can subsequently be subtracted from the measured antisymmetric port signal. The remaining uncertainty is proportional to the calibration uncertainty at the time of the measurement multiplied by the amplitude of the applied calibration signal.

6.1 Swept Sine

Swept sine calibration is best suited for calibrations between data runs. During such a calibration run a sine wave displacement signal is applied to one of the test masses when the interferometer is locked. The frequency is then slowly swept over the gravitational wave detection band measuring the error signal at the antisymmetric port as function of the displacement. This directly determines the closed loop transfer function as given in eqn. (31). Since the detector is off-line the signal-to-noise ratio of the calibration signal can be large and the measurement time can be kept short.

6.2 Fixed Frequency Calibration Lines

A fixed frequency calibration line allows to monitor short-time gain fluctuations. A calibration line below the unity gain frequency of the differential arm length servo is mostly sensitive to gain changes of the suspension controller, whereas a calibration line above the unity gain frequency will monitor both the optical and the sensor gain. One could try to subtract the calibration line from the data, but it is unlikely that the calibration frequencies will still carry convincing information about gravitational waves. By giving up the information at the calibration frequencies the amplitude of the displacement signal can then be made large compared to the noise and, hence, gain fluctuations can be monitored on very short time scales (~seconds).

6.3 Wide-Bandwidth Pseudo-Random Signal

Adding a pseudo-random displacement signal to a test mass with an amplitude well below the noise level avoids the disadvantages of the fixed frequency calibration lines by distributing the energy over the whole gravitational wave band. Since the disturbances of the system are small and without any frequency preferences the degradation of the gravitational wave sensitivity is negligible for all practical purposes. Furthermore, the calibration stretches over the whole band at once and by using different pseudo-random series, in principle, all four test masses can be

actuated independently to give a simultaneous calibration of both arms. Since the maximum amplitude of the added signal is preferable below the noise level, a certain amount of integration time (usually between several minutes and a few hours) is required to extract the calibration signal.

6.3.1 Generating a Pseudo-Random Calibration Signal

The generation of the pseudo-random signal is schematically shown in Fig. 8. A random generator generates a random sequence of zeros and ones at the sampling frequency which is first band-pass filtered to select the calibration signal bandwidth and which is then filtered with the GW-sensitivity transfer function to give a constant signal-to-noise ratio over the whole bandwidth. Finally, the gain is adjusted to yield the needed displacement signal.

6.3.2 Extracting the Calibration Information

If we denote the displacement signal induced by the pseudo-random calibration signal as Φ_{ps} and the measured antisymmetric port signal due to this signal and an additional noise term as $S_{ps} + S_n$, one can approximate the gravitational wave transfer function by

$$GW_{cal}(f_0) \approx \frac{1}{\Delta f} \int_{f_0 - \Delta f/2}^{f_0 + \Delta f/2} \frac{S_{ps}(f) + S_n(f)}{\Phi_{ps}(f)} df \tag{38}$$

where Δf is the calibration bandwidth. Using eqn. (31) one finds

$$GW_{cal}(f_0) \approx \frac{1}{\Delta f} \int_{f_0 - \Delta f/2}^{f_0 + \Delta f/2} GW(f) \left[1 + \frac{\Phi_n(f)}{\Phi_{ps}(f)} \right] df \tag{39}$$

The calibration error is then solely determined by the second term in eqn. (39). If the total calibration time is denoted by T, the number of independent frequencies within the calibration

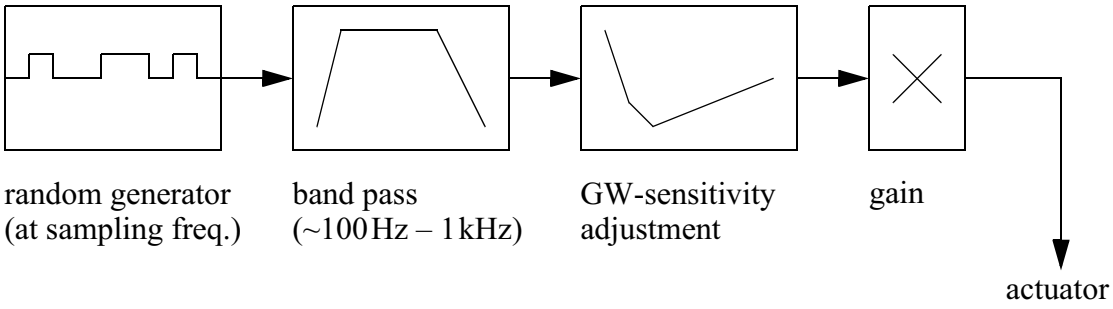

Figure 8: Pseudo-random signal generation.

bandwidth is given by $T\Delta f$. Using $R_{S/N}$ for the signal-to-noise ratio between the $\Phi_{ps}(f)$ and $\Phi_n(f)$ one can approximate the calibration error by

$$\frac{\Delta GW_{cal}(f_0)}{GW_{cal}(f_0)} \approx \frac{e^{i\alpha}}{R_{S/N}}\sqrt{\frac{1}{T\Delta f}} \tag{40}$$

where α is a random phase. Finally, we calculate the individual gain and timing errors:

$$\left|\frac{\Delta GW_{cal}(f_0)}{GW_{cal}(f_0)}\right| \approx \frac{1}{R_{S/N}}\sqrt{\frac{1}{2T\Delta f}} \quad \text{and} \quad \Delta t\left(\frac{\Delta GW_{cal}(f_0)}{GW_{cal}(f_0)}\right) \approx \frac{1}{2\pi f_0 R_{S/N}}\sqrt{\frac{1}{2T\Delta f}} \tag{41}$$

Requiring a gain error of 1% or less, a signal-to-noise ratio of $R_{S/N} \approx 1$ and a calibration bandwidth of $\Delta f \approx 1\,\text{Hz}$, the measurement time for the calibration becomes $T \geq 90\,\text{min}$. The corresponding timing error at $f_0 = 100\,\text{Hz}$ is then $\Delta t \approx 15\,\mu\text{sec}$. As can be seen from these numbers reducing the signal-to-noise ratio to a more favorable 10%, would increase the measurement time by two orders of magnitude, i.e. beyond practical limits. Of course, a high signal-to-noise ratio of order unity will require that the calibration signal has to be subtracted from the measured antisymmetric port signal before proceeding with the gravitational wave analysis.

7 Error Analysis

The error analysis is divided into actuation uncertainties, the uncertainties in determining the interferometer response function and the statistical measurement error.

7.1 Actuation Uncertainties

The uncertainties of a photon actuator can be directly derived from eqn. (35); an estimate is presented in Table 1. The largest uncertainty will be in the measurement of the absolute laser power.

Table 1: Actuation Uncertainties.

Description	variable	nominal value	estimated error	unit
Laser power	P	1 – 100	1%	mW
Test mass	M	10	0.001[1]	kg
incident angle	α	0 – 0.1	0.01	rad
Speed of light	c	299792458	0	m/s
Frequency	ω_c	50 – 1000	negligible	Hz
Arm cavity length	L	4000	0.01	m

1. Air pressure correction of order 8 g.

Neglecting the angular dependence of the gravitational wave signal the gravitational wave strain is related to the displacement by eqn. (37). Since the arm cavity length is known within $\pm 1\,\text{cm}$, its

contribution to the total error is not significant. The crosscoupling of the small Michelson length into the gravitational wave signal was estimated in eqn. (30) to be negligible.

7.2 Response Function Uncertainties

Calibrating the antisymmetric port signal by means of eqn. (31) will then give a relation between the measured signal and the gravitational wave strain. Fluctuations in the interferometer or the servo compensation can lead to additional uncertainties. We estimate these fluctuations by taking the derivative eqn. (31) in respect to the optical gain K_I and in respect to the (suspension) controller gain K_P. To further simplify the calculations we assume

$$I(s) = \frac{1}{1 + s/\omega_{cav}}, \quad P(s) = 1 \quad \text{and} \quad G(s) = \frac{\omega_{BW}(1 + s/\omega_{cav})}{s}. \tag{42}$$

where the unity gain frequency is at $\omega_{BW}/2\pi$. Using $K_I = K_P = 1$ we then obtain

$$\frac{\Delta GW(s)}{GW(s)} = \frac{s}{\omega_{BW}(1 + s/\omega_{BW})}\Delta K_I - \frac{1}{1 + s/\omega_{BW}}\Delta K_P \tag{43}$$

From the above eqn. one can see that the optical gain error dominates above the unity gain frequency, whereas the controller gain error dominates below the unity gain frequency. Fig. 9 shows the relative contribution of an error in the optical gain and in the controller gain, respectively, to the gain error and timing error of the calibration function. As can be seen fluctuations of K_I and K_P have to be monitored to better than 0.5%, in order to not deteriorate the overall calibration accuracy of 1% in gain and 10µsec in time.

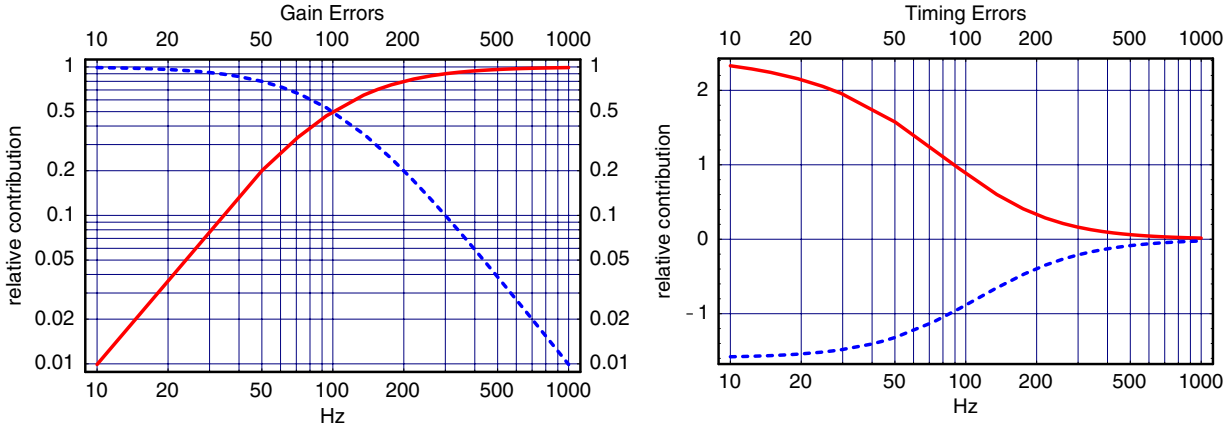

Figure 9: Relative contribution of an error in K_I (solid curve) and K_P to the gain error (left) and to the timing uncertainty. The unity gain frequency was chosen at 100 Hz.

7.3 Internal and Violin Resonances

Internal resonances of the test masses and violin modes of the suspension wires will produce distinct peaks in the interferometer actuation response function. Phase shifts and gain changes due

to these resonances should be well contained around the resonance frequencies, since their Q is extremely high. To improve the calibration accuracy for nearby frequencies one can try to fit and subtract the resonance line from the final calibration spectrum. Of course, in some very narrow bands around the resonance frequencies the calibration information will not be reliable, but it won't be needed there in the first place.

7.4 Measurement Error

Since statistical errors depend on the signal-to-noise ratio of the calibration signal and inversely on the square root of the measurement time, it is most likely possible to make the integration time long enough to keep the statistical errors well below the systematic ones. When calibration changes have to be monitored on short time scales — i.e. minutes — one can make sure that the signal-to-noise ratio is sufficiently large to begin with. Therefore, the statistics should never be the limiting uncertainty.

8 Conclusions

We have shown that a calibration precision of ~2% in the gravitational wave strain amplitude and ~10 μsec in the determination of the arrival time is both experimentally feasible and physical sensible to extract the available gravitational-wave information given the initial LIGO sensitivity.

References

[1] B.F. Schutz, Nature **323** (1986), 310.

[2] B. Allen, *"LIGO calibration accuracy"*, LIGO-T960189-00-E.

[3] C.W. Misner, K.S. Thorne and J.A. Wheeler, *"Gravitation"*, W.H. Freeman & Co. (San Francisco) 1973.

[4] J.-Y. Vinet, B. Meers, C.N. Man and A. Brillet, Phys. Rev. **D38** (1988), 433.

[5] R. Schilling, Class. Quantum Grav. **14** (1997) 1513-1519.